Porphyry gold system of Beluj in the mantle of the Štiavnica stratovolcano (Slovakia)

Jaroslav Kozák[1], Peter Koděra[1], Jaroslav Lexa[2], František Bakos[3], Levente Molnár[4], Markus Wälle[5]

[1] Department of Geology of Mineral Deposits, Faculty of Natural Sciences, Comenius University in Bratislava, Ilkovičova 6, 842 15 Bratislava, Slovakia; kozakminerals@gmail.com, kodera@fns.uniba.sk
[2] Earth Science Institute of the Slovak Academy of Sciences – Geological Division, Dúbravská cesta 9, 840 05 Bratislava, Slovakia; jaroslav.lexa@gmail.com
[3] GREEN VIEW s.r.o., Nevädzová 5, 821 01, Bratislava, Slovakia; fbakoss@yahoo.com
[4] Nám. Priateľstva 2172/33, 929 01 Dunajská Streda, Slovakia; luismoloar@gmail.com
[5] Department of Earth Sciences, ETH Zürich 8092, Zürich, Switzerland; mwalle@mun.ca

AGEOS

Abstract: Beluj magmatic-hydrothermal centre is a small porphyry gold occurrence related to an andesite/diorite porphyry intrusion, located in the mantle of the Štiavnica stratovolcano in the Central Slovakia Volcanic Field. The upper part of the intrusion is affected by K-silicate alteration (biotite, magnetite, K-feldspar) that is in deeper parts accompanied by Ca-silicate alteration (actinolite). Intermediate argillic alteration overprint (smectite, illite, chlorite ± calcite, chabasite) is locally more intensive and can be geochemically modeled by decreased Na/Al ratio. The youngest advanced argillic alteration (kaolinite, dickite, pyrophyllite) occurs at margins of the intrusion. Gold mineralization is spatially associated with a quartz stockwork, including magnetite-biotite (EB-type), A- and B-type quartz veinlets. Native gold grains of high fineness (891–951) were found in smectite in cavities of a banded quartz veinlet. Rare sulphide minerals (mostly pyrite and rare chalcopyrite) usually occur in cavities in quartz. Quartz vein hosts abundant vapor inclusions, some CO_2- and Cu-enriched and rare Au-bearing Fe-K-Na-rich salt melt inclusions with various daughter minerals and homogenization temperatures >600°C. Oxygen isotope composition of vein quartz and magnetite indicates equilibrium with hot fluids (570/650°C) of magmatic origin. Alteration patterns, mineralogy and fluid properties at the Beluj occurrence are similar to porphyry gold systems in the Javorie stratovolcano. However, the hydrothermal system was quite small, which had a negative consequence on economic value of this locality.
Key words: porphyry, gold, Beluj occurrence, Štiavnica stratovolcano, salt melt, Raman spectroscopy, LA-ICPMS, fluid inclusion

1. INTRODUCTION

The porphyry gold mineralization near Beluj village is a small uneconomic occurrence of porphyry gold type ore, located in the mantle of the Štiavnica stratovolcano. This type of mineralization is a relatively new in the Western Carpathians, discovered by EMED Slovakia Ltd. on several localities in the Central Slovakia Volcanic Field during the years of 2006–2009. Porphyry gold mineralization was found here on seven localities within two stratovolcanoes, including the economic deposit of Biely Vrch in the Javorie stratovolcano (Bakos et al., 2010; Hanes et al., 2010) .

In general, porphyry gold deposits are a relatively new type of gold deposits that become more important and economically significant. The absence of copper in mineable concentration is typical (<0.15 wt %; Sillitoe, 2010) while gold concentrations on the economically significant deposits are from 0.8 to 2 ppm Au (Sinclair, 2007). Gold rich porphyry deposits are usually formed in shallow parts of the crust (1–2 km; Cox & Singer, 1988). The recent microanalytical study of the Biely Vrch deposit showed that this deposit and probably similar porphyry gold systems worldwide too, formed from nearly anhydrous Fe-K-Na-Cl salt melts containing ~10 ppm Au but negligible Cu, coexisting with hydrous vapor of very low density (Koděra et al., 2014). This exceptional fluid evolution requires an Fe-rich, high-K calc-alkaline source magma that may have been enriched in Au due to a preceding subduction metasomatism and was partially melted in an extensional setting (Koděra et al., 2014). Shallow subvolcanic emplacement of hydrous magma enabled exsolution of vapor and hypersaline liquid at high temperature (~850 °C). During ascent to the level of the intrusion hosting the ore (0.5–1 km), fluid expansion at high temperature but low pressure leads to NaCl crystallization and further water loss to the vapor, generating an increasingly Fe-K-rich salt melt. The low sulphur fugacity, resulting from fluid expansion, suppressed precipitation of sulphides, explaining the gold-only enrichment in this rare type of gold ore (Koděra et al., 2014).

The Beluj hydrothermal system was first time discovered during regional geological mapping of the Štiavnica stratovolcano (Konečný et al., 1977). Historical vertical drillhole KB-1/330.3 m was set in very middle of the parental intrusion and stopped within it, but did not find any significant mineralization. The intrusion was reported to be a stock of hornblende-hypersthene andesite porphyry with rare phenocrysts of quartz and garnet affected by a strong hydrothermal alteration (Konečný et al., 1977). Geophysical exploration in the area of the porphyry intrusion recognized positive gravity and magnetic anomalies surrounded by IP anomalies and alternating zones of high and low resistivity (Filo et al., 1980). In 2009 EMED Slovakia Ltd. carried out two inclined boreholes which detected uneconomic resources estimated at 58.4 Mt ore with 0.3 ppm Au (Bakos et al., 2010). The boreholes were subject to mineralogical research already by Bakos et al. (2010) and later by Molnár et al. (2012). However, both of the studies represented just preliminary studies of limited extent. This paper presents the results of follow up works with new mineralogical and fluid inclusion data that enabled to discuss genesis of this porphyry gold system and to compare it with other porphyry systems in the Central Slovakia Volcanic Field.

Manuscript received: 2016-09-05
Revised version accepted: 2017-06-13

2. GEOLOGICAL SETTING

The hosting Štiavnica stratovolcano is situated in the southern part of the Central Slovakia Volcanic Field. An extensive caldera, a voluminous subvolcanic intrusive complexes and a late-stage resurgent horst in the caldera centre accompanied by rhyolite activity are the most characteristic features (Konečný et al., 1995). According to Konečný et al. (1998) evolution of the Štiavnica stratovolcano occurred in five stages during the interval 15.0 to 11.2 Ma (Chernyshev et al., 2013. Its evolution started with the formation of a large andesite stratovolcano (15.0–13.5 Ma), composed of pyroxene and amphibole-pyroxene andesite including lava flows, extrusive domes, pyroclastic flow deposits and epiclastic breccias. In the central zone, numerous sills and laccolites of pyroxene and amphibole-pyroxene andesites and andesite porphyries were emplaced mainly in basal parts of the stratovolcanic complex. At the same time several andesite/diorite porphyry intrusions were emplaced into stratovolcanic complexes (mantle) surrounding the central zone, some of them hosting porphyry gold mineralogical occurrences, including the mineralization in the Beluj site (Bakos et al., 2010). During a subsequent break in volcanic activity, evidenced by denudation of the stratovolcano, emplacement of diorite, granodiorite and granodiorite to quartz-diorite porphyry subvolcanic intrusions took place in the central zone (13.5–12.9 Ma). Extrusive activity of biotite-amphibole andesite associated with the caldera subsidence (13.1–12.7 Ma) was followed by renewed pyroxene and amphibole-pyroxene andesite activity during the post-caldera stage (12.7–12.2 Ma). Final long-lasting resurgent horst uplift in the centre of the caldera was associated with rhyolitic volcanic activity (12.2–11.4 Ma).

The lower structural unit (1st stage) of the Štiavnica stratovolcano hosts several porphyry gold occurrences, all located in the stratovolcanic mantle which is surrounding the central zone of the stratovolcano (Fig. 1). The porphyry gold system near the Beluj village is the biggest magmatic-hydrothermal system of this type. The other porphyry gold type localities are known to occur between villages Župkov, Píla and Malá Lehota, but they represent just small mineralogical occurrences without any economic potential (Knésl et al., 2006; Bakos et al., 2010). Non-mineralized intrusive centres of similar composition and setting are also known from Šášovské Podhradie and Prochot north of the caldera fault (Konečný et al., 1998; Bakos et al., 2010).

The Beluj magmatic-hydrothermal system (Fig. 2) is spatially related to a biotite, garnet and quartz bearing amphibole-hypersthene andesite/diorite porphyry stock-like intrusion, passing laterally into a laccolite shaped intrusion of andesite porphyry with intrusive breccias at margins (Konečný et al., 1977; Filo et al., 1980; Bakos et al., 2010). It is probable, that the laccolite in outer parts of the Beluj intrusive complex represent an earlier co-magmatic phase. The intrusive bodies were emplaced into rocks of the 1st pre-caldera stage of the Štiavnica stratovolcano – effusive complex of pyroxene andesites and a complex of hornblende-pyroxene andesite extrusive domes and pyroclastic flow deposits. In the southern part of the locality altered rocks of the intrusive complex are covered by unaltered rocks of the Sebechleby Formation – a stratovolcanic complex of amphibole-pyroxene andesites

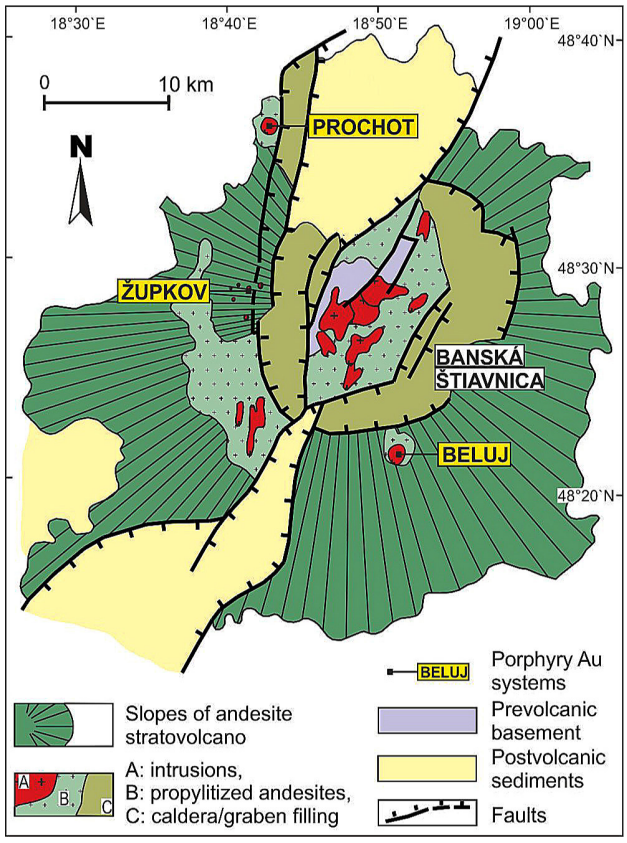

Fig. 1. Schematic map of the Štiavnica stratovolcano with the location of porphyry gold magmatic-hydrothermal systems, including Beluj (after Lexa et al., 1999 and Bakos et al., 2010).

representing the younger part of the 1st pre-caldera stage of the Štiavnica stratovolcano (Konečný et al., 1977, 1998). Remnants of a much younger biotite-amphibole-pyroxene lava flow of the Sitno effusive complex rest on the northern part of the intrusive complex. Sporadic blocks of alkali basalts indicate a presence of alkali basalt dikes.

The intrusion is affected by several types of hydrothermal alteration with variable spatial distribution (Konečný et al., 1977; Bakos et al., 2010). High temperature alterations of the stock-like intrusion (K-feldspar, biotite, magnetite, actinolite) grade outward into zones of intermediate argillic alteration and propylitization, affecting older rocks to the distance of 3 km. Younger advanced argillic alteration occurs in zones of the NW–SE orientation (Fig. 2; Bakos et al., 2010). However, the interpreted orientation is questionable as it does not correspond to the orientation of low resistivity zones indicated by geophysical measurements (Filo et al., 1980). The alterations are accompanied by hydrothermal veinlets of several generations. The most abundant are quartz veinlets forming quartz stockwork that is accompanied by gold mineralization (Bakos et al., 2010). The BVE-1 borehole crosscut also two zones of hydrothermal-explosive inter-mineralization to post-mineralization breccias. Breccias in the interval 118 to 140 meters are fine grained of the pebble-dike type with rock-flour matrix. It is affected by silicification and biotitization and contains older fragments of quartz veins. Breccia in the interval 218 to 230 meters is affected by intense silicification, biotitization,

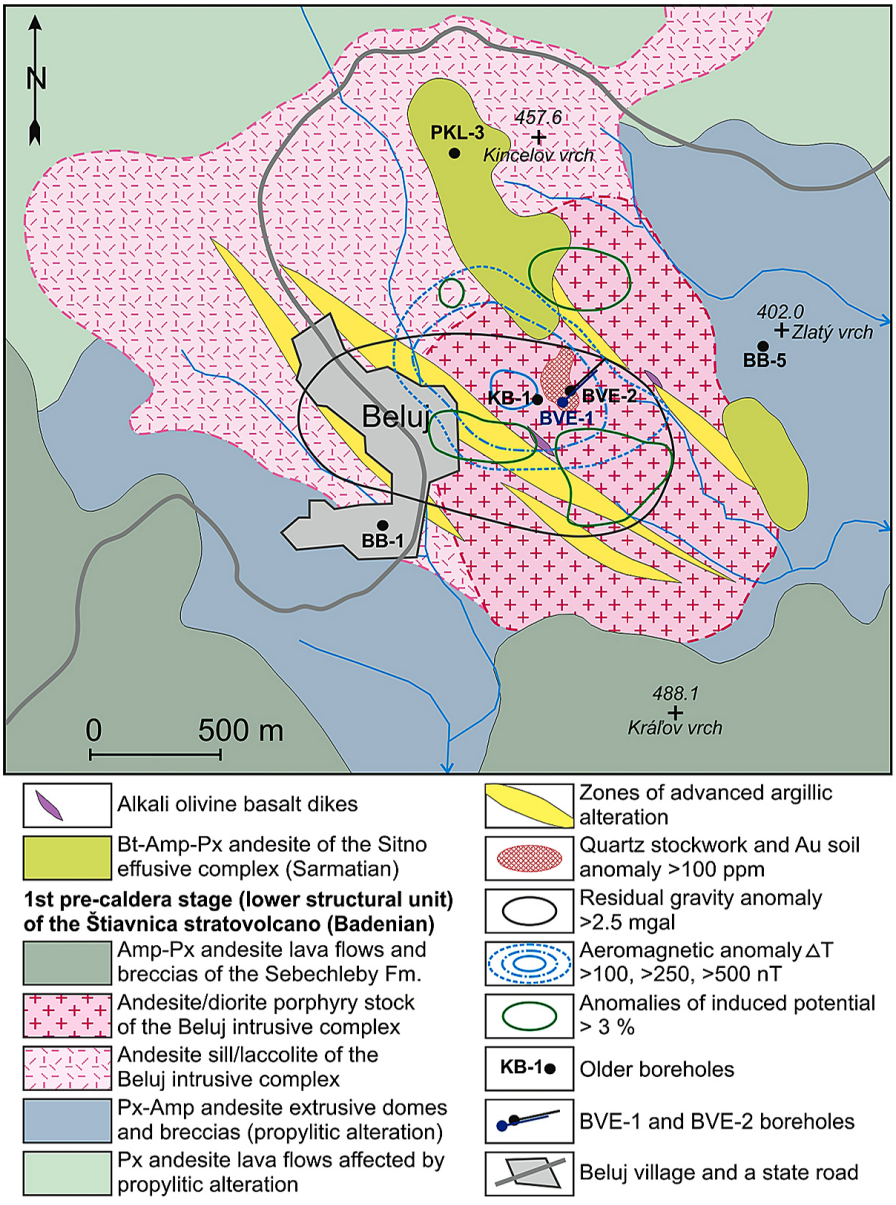

Fig. 2. Structural scheme of the Beluj magmatic-hydrothermal system, based on the geological map of Konečný et al. (1977), geophysical maps of Filo et al. (1980) and alteration map of Bakos et al. (2010).

and intermediate argillic alteration (Bakos et al., 2010; Molnár et al., 2012).

3. METHODS

Whole rock geochemical data and core logs from BVE-1 and BVE-2 drillholes used in this study were provided by EMED Slovakia, Ltd. (analytical conditions are in Hanes et al., 2010). Geochemical data were used for geochemical modelling of alteration zones, based on concentrations of selected representative elements (all element ratios are based on wt. % contents). Laboratory evaluation was performed on representative samples of hydrothermal alteration, veinlets and gold mineralization, including transmitted and reflected polarized light microscopy, XRD, microprobe, fluid inclusion and oxygen isotope study.

Microprobe analyses (WDS, EDS, BSE and CL imaging) of gold and associated alteration minerals were carried out on the electron microprobe CAMECA SX 100 at the State Geological Institute of Dionýz Štúr in Bratislava at standard conditions. Cathodoluminiscence (CL) imaging combined with Ti in quartz (TitaniQ) geothermometry (Thomas et al., 2010; Huang & Audétat, 2012) were used on selected samples of vein quartz to determine relative age and formation temperatures of mineralization and hydrothermal alteration in the vicinity of veinlets. Combination of the geothermometry with CL imaging is particularly useful because the intensity of cathodoluminiscence emission of vein quartz in porphyry systems mostly depends on concentration of Ti in quartz, which is mainly a function of temperature (Rusk et al., 2008). Precise analyses of Ti for the application of the TitaniQ geothermometer were measured at current 180 nA simultaneously on two spectrometers in 5 cycles, each lasting 1 minute, resulting in the detection limit ~8 ppm Ti.

Non-oriented specimens for the whole rock XRD analyses were prepared by mixing 1 g of rock (fraction <0.25 mm) with 250 mg of Al_2O_3 (internal standard) and 4 ml of distilled ethanol. Prepared mixture was milled by electrical mill McCrone Micronizing Mill (Środoń et al., 2001). XRD powder analyses of whole rock samples were realized on diffractometer Philips PW 1710 using Cu Kα radiation at the Slovak Academy of Sciences in Bratislava and on diffractiometer Bruker D8 Advance at the Department of Mineralogy and Petrology at Comenius University in Bratislava. Measurement interval 4-65°2θ was used with the step 0.02°2θ in 0.8-2 s. XRD spectra DiffracEva and X´Pert software were used for qualitative evaluation of spectra. RockJock (Eberl, 2003) and TOPAZ softwares were used for subsequent quantitative evaluation of spectra.

Mineral composition of rocks based on XRD whole rock analyses and borehole geochemical analyses (2 meters sections – provided by EMED Slovakia, Ltd.) were used for geochemical modelling of alteration patterns. A set of correlation diagrams was constructed that enabled to interpret changes in chemical and mineral composition of rocks due to the effect of hydrothermal alteration. Changes in concentrations of major alkali elements were normalized to concentration of the immobile aluminium to

avoid the effect of variability in chemical composition of the former fresh magmatic rock. Correlation diagrams were interpreted in comparison to chemical composition of unaltered porphyry at the Beluj site, available from the database of chemical analyses of rock complexes of the Štiavnica stratovolcano (Lexa et al., 1997).

Fluid inclusions were studied in thin sections and in doubly polished wafers (~200 μm thick). The observed inclusions were assigned a probable primary or secondary origin according to the criteria of Roedder (1984). The microthermometric behaviour of fluid inclusions was studied in doubly polished wafers on Linkam THMSG-600 stage at the Department of Earth Sciences at ETH Zürich and at the Department of Geology of Mineral Deposits, Comenius University in Bratislava. The equipment was calibrated with natural fluid inclusions with pure CO_2 (-56.6 °C), pure water (0 °C), and inorganic standards (e.g., $K_2Cr_2O_7$, 371 °C). Raman spectroscopy of fluid inclusions were realized on LabRamHR 800 (HORIBA JOBIN-YVON) equipped with an Olympus BX41 optical microscope in the laboratory of Earth Science Institute of the Slovak Academy of Sciences in Banská Bystrica. A polarized laser emission at λ=532 nm (frequency-doubled Nd:YAG laser) was used for excitation. The Raman-scattered light was collected in 180° geometry through a 100x objective lens with numerical aperture 0.8 and dispersed by diffraction grating with density 1800 gr/mm onto a Peltier cooled CCD detector Synapse (Horiba Jobin-Yvon). Spectra were collected in 2 acquisitions of 120 seconds in range 50–4000 cm^{-1}.

LA-ICP-MS analyses of vapour and salt melt inclusions were performed at the Department of Earth Sciences at ETH Zürich (ETH-GeoLas 193 nm Excimer Laser system, Elan 6100 quadrupole ICPMS; Günther et al. 1998; Heinrich et al., 2003), with quantification of analytical signals using the program SILLS (Guillong et al., 2003). Concentration of salt melts was calculated assuming the total of the main salts is 100% ($NaCl+KCl+FeCl_2+CaCl_2+MnCl_2$). Concentration of salts in vapours was calculated assuming the total of salts is 1 %. However, the exact salinity of vapour inclusions is not known therefore the real concentration in inclusions could be significantly higher or lower than that calculated here.

Oxygen isotope compositions of monomineral separates were analysed at the Scottish Universities Environmental Research Centre in Glasgow. For $^{18}O/^{16}O$ measurement, 1 mg of oxygen bearing samples reacted with chlorine trifluoride using laser heating. The oxygen isotope laser fluorination technique has been described by Macaulay et al. (2000). Precision of determinations by laboratory replicate analysis is 0.2‰ for $\delta^{18}O$ at 1σ.

List of abbreviations used in this paper: Act – actinolite, Aln – allanite, Amp – amphibole, Ap - apatite, Au - gold, Bn - bornite, Bt - biotite, Cal - calcite, Ccp - chalcopyrite, Chl - chlorite, Cov - covellite, Dic - dickite, Ep - epidote, Fl - fluorite, Grt - garnet, Hbl - hornblende, Ill - illite, Ilm - ilmenite, Kfs - potassium feldspar, Kln - kaolinite, Mt - magnetite, Plg - plagioclase, Prp - pyrophyllite, Py - pyrite, Px – pyroxene, Qtz - quartz, Sm - smectite, Sph - sphalerite, Ttn - titanite, Tur - tourmaline, Zeo – zeolite, IA - intermediate argillic, AA - advanced argillic, LT - low temperature, HT - high temperature, SM - salt melts, XN – crossed nicols optical image, BSE – backscattered electron image.

4. RESULTS

4.1. Host rocks

Former magmatic host rock is very rarely preserved. Relics of host rocks were observed in the lowest parts of BVE-2 borehole (Fig. 3a). Spatially this presents outer part of the hydrothermal system. The intrusion is formed by amphibole-hypersthene andesite/diorite porphyry. Phenocrysts of plagioclase, hypersthene and amphibole (ferrohornblende - magnesiohornblende) are accompanied by rare phenocrysts of resorbed quartz, biotite, garnet (andradite, almandine-pyrope) and/or augite (Fig. 4a). Rarely,

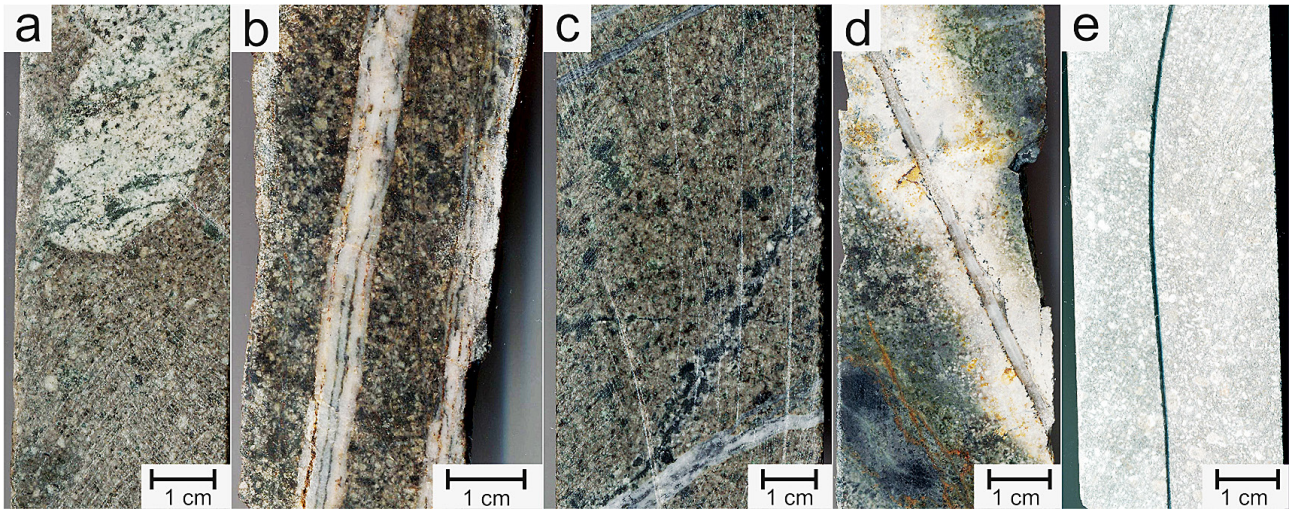

Fig. 3. Macrophotographs of typical andesite porphyry, alteration patterns and quartz veinlets in cores from the BVE drill holes: A – a relatively fresh andesite porphyry hosting a xenolite of diorite porphyry (BVE-2/253.5); B – K-silicate alteration including banded quartz veinlets (BVE-1/29.6); C – intermediate argillic alteration overprinting K-silicate alteration with early biotite-magnetite±quartz veinlet cut by late banded quartz veinlet (BVE-2/127.1); D – white kaolinite halo in the vicinity of a late quartz veinlet related to advanced argillic alteration (BVE-1/244.3); E – advanced argillic alteration (BVE-2/236.8).

in biotite phenocrysts micron-size inclusions Cu-sulphides (bornite, chalcopyrite) were observed, probably representing trapped magmatic sulphide melts (Fig. 4b). Groundmass is typically holocrystalline and grainy with microaplitic, or less often microlitic-microaplitic or microlitic-micropoikilitic texture (Konečný et al., 1977). Northern part of the intrusion is characterized by

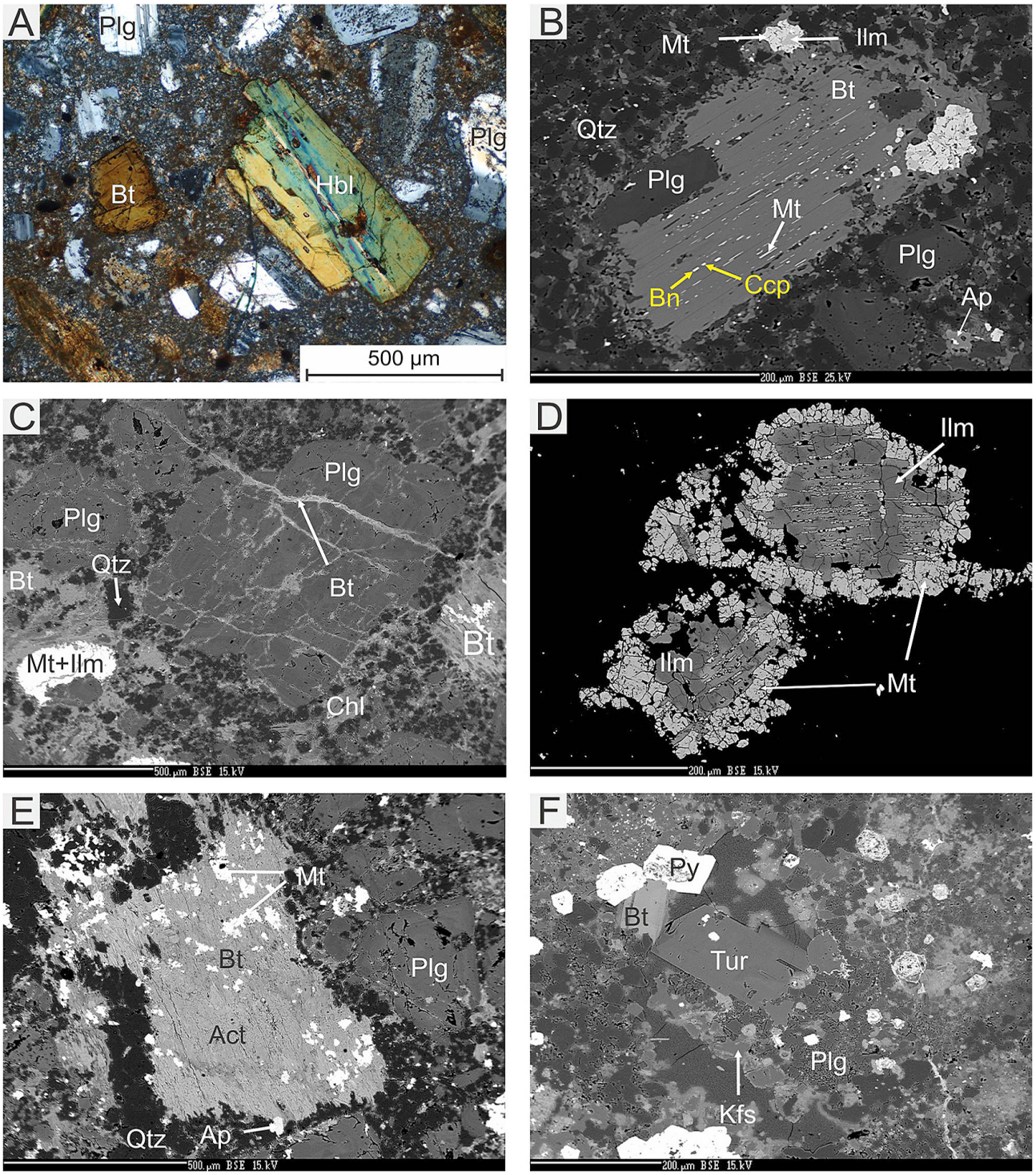

Fig. 4. Microphotographs of fresh andesite porphyry and rocks affected by high temperature hydrothermal alteration: A – fresh andesite porphyry with phenocrysts of hornblende, biotite and plagioclase in matrix composed mostly of quartz and plagioclase (BVE-2/253.5; XN) ; B – biotite phenocryst with numerous tiny inclusions of bornite and chalcopyrite suggestive of sulphide melt inclusions (BVE-1/229.2; BSE); C – K-silicate alteration with secondary biotite and magnetite, including biotite veinlets intersecting a plagioclase phenocryst (BVE-2/92.0; BSE); D – Ilmenite overgrown by magnetite from K-silicate alteration (BVE-1/139.1; BSE); E – Former mafic magmatic phenocryst replaced by a mixture of actinolite, biotite and magnetite representing mixed K- and Ca-Na silicate alteration (BVE-1/139.1; BSE); F – mixed K- and Ca-Na silicate alteration including K-feldspar, biotite, plagioclase, accompanied by isometric crystals of magnesiofoitite tourmaline and pyrite (BVE-1/244.3)

lack of garnet, quartz and biotite with holocrystallic-microlitic to microlitic-microaplitic texture of rock. Groundmass textures are overprinted variably by silicification.

4.2. Hydrothermal alteration

Magmatic-hydrothermal centre of the Beluj occurrence is affected by several types of hydrothermal alterations. Alterations can be roughly divided into older higher temperature alterations, younger lower temperature alterations and post-mineralization advanced argillic alteration type.

4.2.1. High temperature alteration

The upper part of the parental intrusion is affected by high-temperature K-silicate hydrothermal alteration (Figs. 3b, 4c, 4d). This alteration type is represented by biotitization and magnetitization of former mafic minerals. Magmatic plagioclases are replaced by hydrothermal K-feldspars. Content of albite component in K-feldspars (orthoclase) varies from 2 to 19 % of Ab, in one case up to 36 % of Ab in the deeper part of hydrothermal system (Table 1). Hydrothermal biotites have decreased content of fluorine (< 1.20 wt. % of F compared to magmatic 1.81 to 3.31 wt. % of F) and increased Fe/Mg ratio compared to magmatic biotites (Table 1). In the deeper parts of system (>150 m), products of Ca-Na silicate alteration were observed, represented by actinolitization of mafic minerals (Fig. 4e) and replacement of former magmatic plagioclases by hydrothermal Na-plagioclases. Products of Ca-alteration occur frequently together with products of K-silicate alteration (orthoclase, magnetite) that suggests the presence of transitional K/Ca-Na alteration type. Rare grains of tourmaline (foitite-magnesiofoitite) were found to accompany this type of alteration (Fig. 4f). Thin tourmaline needles were also observed in one surface sample and confirmed by XRD whole-rock analyse (Table 2). All types of high temperature alteration are overprinted by low temperature alteration assemblages with variable intensity (Figs. 3c, 5a–c).

High temperature alteration patterns can be geochemically modelled by increased K/Al and Ca/Al values compared to the fresh porphyry (K/Al > 0.16; Ca/Al > 0.53; Fig. 6). Despite the fact that K-feldspar and biotite (as well as illite representing later K-bearing alteration product) were relatively common in most of the studied samples, the K/Al ratio is never significantly increased compared to the fresh rock (Fig. 7) and no apparent correlation exists with the variability of the alteration mineral composition of the rock. Similarly, Ca/Al nor Ca/K ratios are considerably elevated (Fig. 6). Thus it follows that the high temperature alteration is just of a weak intensity at the Beluj intrusive complex, with no apparent effect on chemical composition of the host porphyry.

4.2.2. Low temperature alteration

The most significant low temperature alteration type is intermediate argillic alteration that partially or fully overprints earlier K-silicate and Ca-Na silicate alterations. Intermediate argillic alteration is represented by smectite, illite-smectite, illite, chlorite, epidote (± allanite) and pyrite (Figs. 5a-b) and it

Tab. 1. Representative WDS analyses of silicate magmatic (*in italics*) and hydrothermal alteration minerals from BVE drill holes in Beluj (in wt. %).

Drillhole	BVE-2/253.5	BVE-2/253.5	BVE-1/139.0	BVE-2/203.8	BVE-2/79.0	BVE-2/92.0	BVE-2/74.5	BVE-2/79.0	BVE-1/244.3	BVE-2/79.0	BVE-2/74.5	BVE-2/74.5
Mineral	Actinolite	*Hornblende*	*Biotite*	Biotite	Chlorite	Chlorite	K-feldspar	K-feldspar	Plagioclase	Plagioclase	Tourmaline	Tourmaline
SiO_2	51.85	44.98	41.91	36.86	32.43	38.19	63.90	64.44	62.90	50.12	35.62	35.35
TiO_2	0.23	2.32	1.01	3.65	0.01	0.02			0.01		0.21	0.22
Al_2O_3	5.32	10.23	10.09	13.60	16.21	14.81	18.69	18.49	23.21	31.92	38.67	38.04
FeO	11.04	12.74	13.11	18.27	19.49	19.33	0.02	0.16	0.59	0.31	6.96	7.73
MnO	0.15	0.14	0.17	0.41	0.94	0.36			0.01		0.05	0.05
MgO	16.12	14.42	19.30	12.65	17.46	12.76	0.00	0.02	0.07	0.00	4.40	3.80
CaO	12.75	11.28	0.08	0.07	0.78	1.75	0.09	0.01	3.50	14.69	1.63	1.78
Na_2O	0.83	1.86	0.17	0.26	0.00	0.05	0.39	0.22	8.86	3.19	0.62	0.58
K_2O	0.21	0.45	8.75	8.73	0.13	0.52	15.13	16.52	0.59	0.15	0.05	0.04
BaO							1.76	0.34				
F	0.21	0.00	3.31	0.04	0.00	0.00			0.00		0.00	0.00
Cl	0.10	0.05	0.41	1.30	0.01	0.01			0.00		0.04	0.07
Total	98.82	98.55	98.31	95.85	87.87	87.81	99.97	100.20	99.77	100.43	88.26	87.66
–O=F	0.09	0.00	1.39	0.01	0.00	0.00			0.00		0.00	0
–O=Cl	0.02	0.01	0.09	0.29	0.00	0.00			0.00		0.01	0.01
Total (F,Cl)	98.71	98.54	96.83	95.54	87.47	87.80			99.77		88.26	87.65

often partially or fully destroys former magmatic texture. Rarely, kaolinite replaces plagioclases in intermediate to advanced argillic alteration (Fig. 5c). According to whole-rock XRD analyses (Table 2), smectite is the most common clay mineral, reaching concentrations above 14 wt. % in most samples, with maximum 49 wt. %. Chlorite is also common, but its concentration usually does not exceed 10 wt. %. Illite has a similar content – it was identified in about half of the analysed samples, but only in 4 samples it reaches concentrations >10 wt. %, with max. 46 wt. %.

Intermediate argillic alteration is often accompanied by low-temperature Ca-alteration, characterized by calcite, Ca-zeolite, smectite and rare titanite. However, calcite is not a frequent mineral and it appears only at increased Ca/Na ratios, when plagioclases are preserved just in low amount and Na content is significantly decreased. In general, concentration of plagioclases is a good indicator of intensity of low temperature alteration. This mineral was identified in all analysed samples, while in about half of the samples it had concentrations > 25 wt. %, max. 68 wt. %. The geochemical correlation plots show that the most significant change in composition of altered rock compared to fresh rock is depletion in Na, which is almost always accompanied by a less intensive removal of Ca (Fig. 5). Mineralogically, the depletion in sodium is mirrored by the increased content of all low-temperature alteration minerals (clay minerals + chlorites + calcite). Based on this fact, the higher intensity of low temperature alteration at Beluj can be modelled by using the Na/Al ratio with the threshold value of 0.13 (Fig. 5). As seen in the drill holes geochemical profiles, more intensive intermediate argillic alteration occurs only in some limited, but mostly continuous, sections of the two drill holes (Fig. 6).

4.2.3. Advanced argillic alteration

Advanced argillic alteration represents the youngest type of alteration which occurs as elongated NW–SE oriented zones at margins of the parental intrusion with thickness from several meters to several tens of meters (Bakos et al., 2010). Based on whole rock XRD analyses of the advanced argillic alteration from surface these zones are formed mainly by kaolinite and dickite (Table 2). Central parts of the alteration zones are formed by argillized and silicified breccias with vuggy texture (Bakos et al., 2010). In drill holes, the advanced argillic alteration occurs only as rare thin zones up to 1 m thick, sampled in BVE-1/112.5 m (kaolinite, dickite, pyrophyllite) and BVE-2/236.0 m (pyrophyllite, montmorillonite) (Figs. 3d, 3e). Kaolinite predominantly replaces here plagioclase phenocrysts (Fig. 5c). Because geochemical data from drill holes are taken from 2 m intervals, geochemical modelling could not be applied for this type of alteration.

Tab. 2. Whole rock XRD quantitative analyses (%) of samples from the BVE drill holes and from surface outcrops of hydrothermally altered rocks.

SAMPLE	Qtz	Plg	Act	Kfs	Bt	Mt	I	Sm	Chl	Cal	Py	Kln	Prp	Tur	Grt
BVE-1/19.7	35.0	52.0			3.6			7.5	2.0						
BVE-1/40.5	64.5	10.8			0.6			9.4	0.5	14.2					
BVE-1/112.5	26.4										2.4	66.6	4.7		
BVE-1/139.0	65.1	22.3			7.9	0.8	0.9	2.8	0.2						
BVE-1/163.0	31.0	31.2	2.3	3.0	12.3	0.3	4.0	6.8	7.1		0.1	1.9			
BVE-1/172.4	1.2	68.3	0.3				22.1	6.4	1.7						
BVE-1/175.1	29.0	38.2		2.5	7.5	1.8	10.9	3.5	6.5						
BVE-1/199.4	28.8	32.5			3.1			21.0	14.6						
BVE-1/218.9	35.0	43.6			5.9			14.5	1.0						
BVE-1/221.6	6.5	33.3		30.8	3.4			24.9	1.1						
BVE-1/227.6	33.3	8.5	0.3	5.9	2.1	0.2	18.7	20.9	9.5			0.7			
BVE-1/231.6	19.8	23.1		15.0	5.4			33.4	1.2						
BVE-1/244.3	25.8	62.7			6.6			1.5	3.3						
BVE-1/252.0	29.5	3.4		4.8	0.8		45.9	15.6							
BVE-2/28.4	36.5	31.8		10.4	10.5	2.0	3.9	3.1	1.2		0.1				
BVE-2/42.0	21.2	26.2		2.5			3.3	31.9	12.3				2.5		
BVE-2/100.0	24.5	24.1		2.9			6.7	26.9	4.4	10.4					
BVE-2/165.2	20.4	2.0		0.8			12.4	44.3	6.0	4.2			7.0		
BVE-2/215.1	35.8	22.0		1.4			10.9	13.3	7.9	3.0	2.2		3.5		
BVE-2/253.5								53.3					46.7		
Be-1												100			
Be-2	17.7	31.4					27.9	17.2	5.8						
B-1a	47.4				1.8		25.8	10.1	2.2			12.8			
B-1c	36.7	1.5		6.9	2.8		35.0	2.8						13.7	0.6
B-3a	45.1						26.3	23.6	4.6						

4.3. Veinlets and mineralization

The Beluj magmatic-hydrothermal centre hosts several generations of veinlets that are associated with the hydrothermal alteration types described above. At least 3 generations of quartz veinlets can be recognized here based on drill core logging. The density of veining is variable from weak to up to >30 % of rock volume, locally forming a dense stockwork or filling of cracks

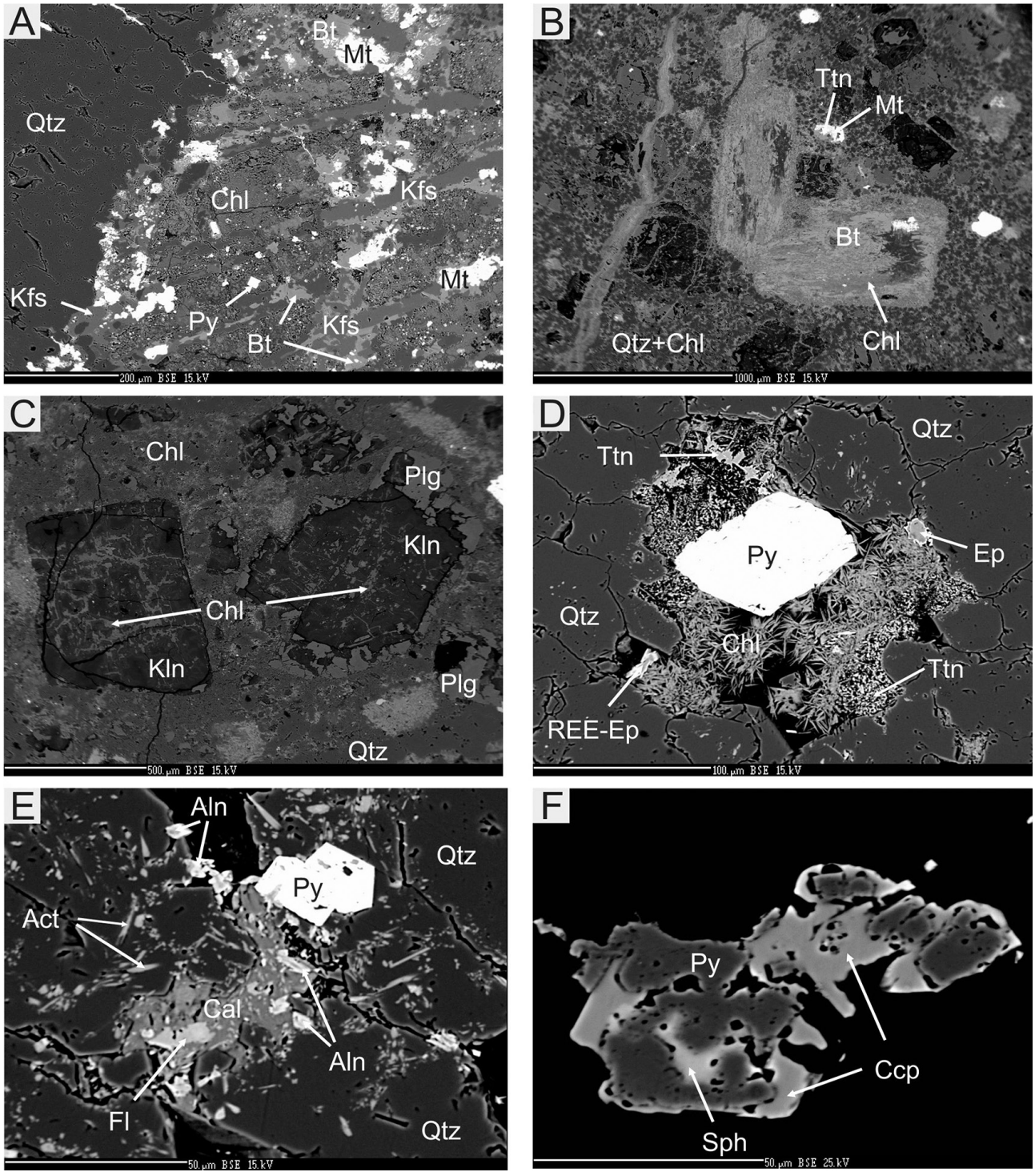

Fig. 5. Backscattered electron images of low temperature hydrothermal alteration and veinlets: A - K-silicate alteration in the vicinity of a quartz veinlet with K-feldspar, biotite and magnetite, partially replaced by intermediate argillic alteration with chlorite and pyrite (BVE-2/127.1; BSE); B – intermediate argillic alteration represented by chlorite replacing biotite phenocryst in quartz-chlorite groundmass and biotite in veinlet (BVE-2/74.5); C – plagioclase phenocrysts replaced by kaolinite in a quartz-chlorite groundmass representing advanced to intermediate argillic alteration (BVE-1/29.6); D – cavity in quartz veinlet filled by chlorite, pyrite, titanite and epidote (BVE-1/187.1); E – cavity in a late quartz veinlet with inclusions of actinolite and filled by calcite, allanite and fluorite (BVE-1/187.1); F – Cluster of sulphide minerals including Fe-rich sphalerite, pyrite and later chalcopyrite in a chlorite veinlet (BVE-1/121.3B).

in hydrothermal breccias (Bakos et al., 2010). The oldest generations of veinlets are EB-type biotite-magnetite±quartz veinlets and more common A-type quartz veinlets, represented mostly by sugary quartz (Figs. 3c, 5b; vein terminology is based on Gustafson & Hunt, 1975). Both types of veinlets are short, discontinuous and with irregular margins, associated with early high temperature K-silicate alteration. Banded (B-type) of quartz veinlets is younger, more common, with dark banding caused by dense accumulations of small vapour inclusions and inclusions of magnetite and/or ilmenite ± chalcopyrite (Figs. 3b, 3c). Bakos et al. (2010) also described scheelite occurring on rims of quartz veinlets. CL imaging showed that quartz in A-veinlets has the strongest luminescence and highest concentrations of titanium (up to 392 ppm Ti; average concentration 95 ppm Ti), while the late banded veinlets show the weakest luminescence and concentrations of Ti mostly below the detection limit (<8 ppm). Central parts of B-type quartz veinlets are filled by chlorite, smectite with increased Fe content, calcite and rare sulphides (Figs. 5d-e). Sulphides, mostly formed by chalcopyrite, pyrite and sphalerite, also occur as discontinuous veinlets that are probably of the same age or younger than B-type quartz veinlets. The youngest generations of veinlets are chlorite (mostly chamosite), calcite and quartz-calcite veinlets, locally with actinolite, fluorite, smectite (nontronite) and sulphide minerals (Figs. 5e, 5f). Late Ca-chabasite veinlets with smectite (nontronite) are also present.

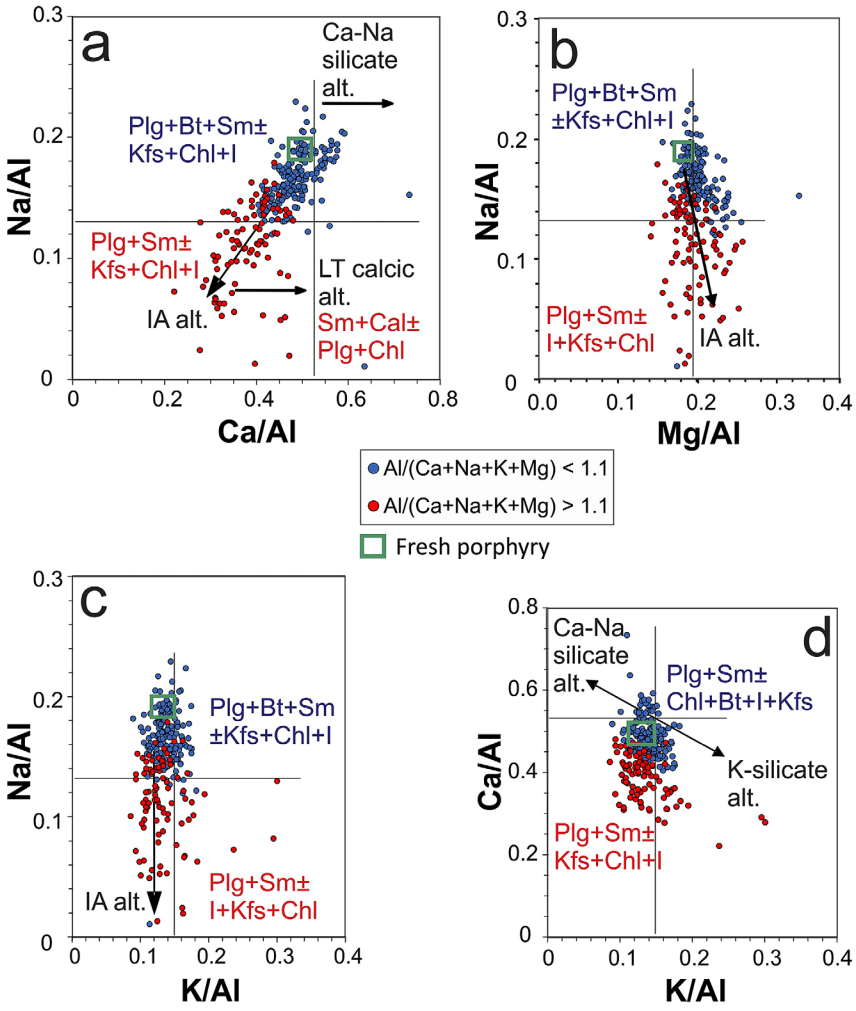

Fig. 6. Geochemical correlation diagrams of selected element wt. % ratios, normalized to aluminium which is normally immobile. Also shown is the average composition of fresh porphyry (Lexa et al., 1997). Thin lines represent element ratios in fresh andesite porphyry. Analyses are separated into two groups according to the ratio of Al to the total of main rock-forming cations (except of Fe), which shows the relative intensity of removal of these elements due to alteration. Main mineral assemblages shown are based on whole-rock XRD analyses. Arrows indicate interpreted trends and relative intensity of hydrothermal alterations.

Gold mineralization in BVE-1 and BVE-2 drill holes is of low and irregular grade from 0.01 ppm up to 1.19 ppm Au. Maximum thickness of Au 0.7 ppm interception was 24 m (Bakos et al., 2010). Gold (and copper) are spatially related to the presence of the quartz stockwork (Fig. 7). Gold concentrations weakly correlate with Cu grades, that reach up to 200 ppm. Silver contents are mostly below detection limit (0.5 ppm; Bakos et al., 2010). There is no clear correlation of Au and Cu contents with a particular type of alteration, as seen in plots of concentrations along holes with geochemical indicators of alteration (Fig. 7).

Native gold grains were found in sample BVE-1/229.2 m in cavities of a banded quartz veinlet. Four gold grains, all having isometric shape and 2 to 5 μm in diameter, occurred in smectite, associated with earlier Ca-zeolite, magnetite, unknown Fe-oxihydroxide and rare covellite. CL imaging and Ti analyses showed, that the quartz vein consisted here of two generations of quartz, while the earlier quartz had high Ti content (>100 ppm) the later, probably associated with filling of cavities with gold, had low Ti content (<8 ppm Ti; Fig. 8e). The host rock of the veinlet is affected by potassic alteration, partially replaced by intermediate argillic alteration (Fig. 8). Bakos et al. (2010) describe gold grains in sample BVE-1/226.6 m hosted directly in a quartz, located on margin of a quartz veinlet, where quartz was intergrown with biotite, partially replaced by a clay mineral. Microprobe analyses of the smectite-hosted gold showed that all gold grains were chemically homogeneous with fineness ranging from 891 to 951 (Table 3). Silver is the only significant accompanying metal with concentrations from 4.36 to 9.25 wt. %.

Sulphide minerals at Beluj are represented mainly by pyrite and pyrrhotite. Pyrite is mostly present as dense impregnations of small pyrite grains of isometric shape in rocks affected by intermediate argillic alteration. Pyrite also occurs in cavities

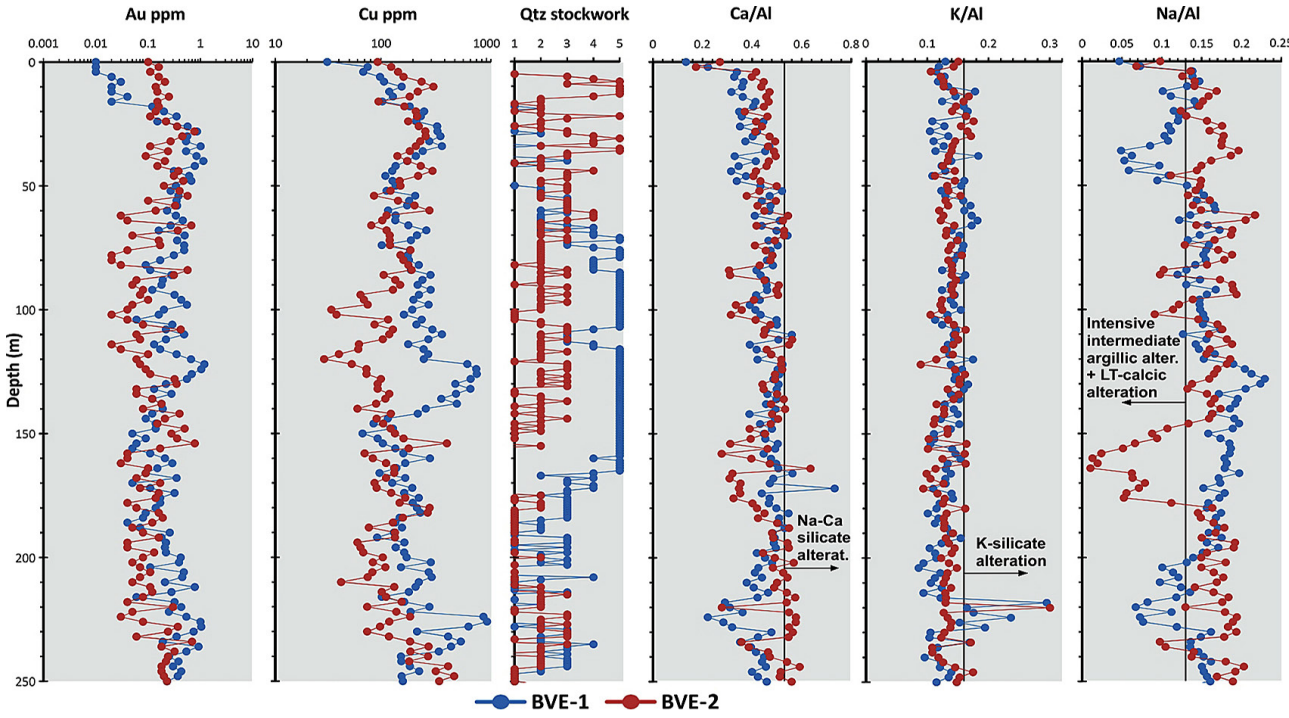

Fig. 7. Whole rock concentrations of Au and Cu, relative abundance of quartz veinlets (data from drill core logging with intensity scale 0 – 5) and Ca/Al, K/Al and Na/Al wt. % ratios from the drill holes BVE-1 and BVE-2. Vertical lines represent threshold values for individual types of hydrothermal alteration (see text for details).

Tab. 3. Representative WDS analyses of gold, bornite and sphalerite from BVE drill holes in Beluj (in wt. %).

Drillhole	BVE-1/229.2	BVE-1/229.2	BVE-1/229.2B	BVE-1/229.2B	BVE-1/121.3B
Mineral	Gold	Gold	Gold	Bornite	Sphalerite
Au	88.19	95.05	89.32		
Ag	9.09	4.36	7.01	0.02	0.03
Cu	0.88	0.41	0.05	62.40	1.55
Hg	0.08	0.08	0.07		0.00
Fe				10.84	6.54
Zn					57.87
Cd					0.48
S				25.99	33.61
As				0.00	
Total	**98.26**	**99.91**	**96.80**	**99.26**	**100.14**

of quartz veinlets or it also forms individual veinlets. Microprobe analyses showed that pyrite grains were chemically homogeneous without any significant accompanying elements. Pyrrhotite was found in rocks affected by intermediate argillic alteration in former biotite phenocrysts and it associates with titanite and rutile. Neither pyrrhotite contains any significant accompanying elements. Chalcopyrite was mostly found in the form of inclusions in quartz veinlets and in intermediate argillic altered rock in smectite and chlorite. Pyrite and chalcopyrite are accompanied by rare other sulphides (sphalerite, galena, chalcopyrite, bornite). Sphalerite is older than chalcopyrite (Fig. 5f) and has increased concentration of Fe (~ 6.5 wt. %, Table 3). Galena was found as very rare small grains only. Rare bornite grains accompany chalcopyrite in banded quartz veinlets. Several grains of native copper of very high fineness (up to 990) were identified in argillic and zeolite veinlets. Furthermore, Bakos et al. (2010) described from altered drill core at Beluj unknown Cu-S (chalcotite, digenite?) and Cu-Fe-S (bornite?) phases. They also described here a common presence of micron-size molybdenite impregnations and rare grains of unidentified Te-Bi minerals.

4.4. Fluid inclusions

Microscopic study of quartz veinlets determined the presence of three basic types of fluid inclusions – vapour inclusions, salt melt inclusions and aqueous vapour-liquid inclusions (Fig. 9).

Monophase vapour fluid inclusions, with no visible liquid phase on the walls of the inclusions, are the dominant type of inclusions at Beluj. They are of primary but often also of secondary

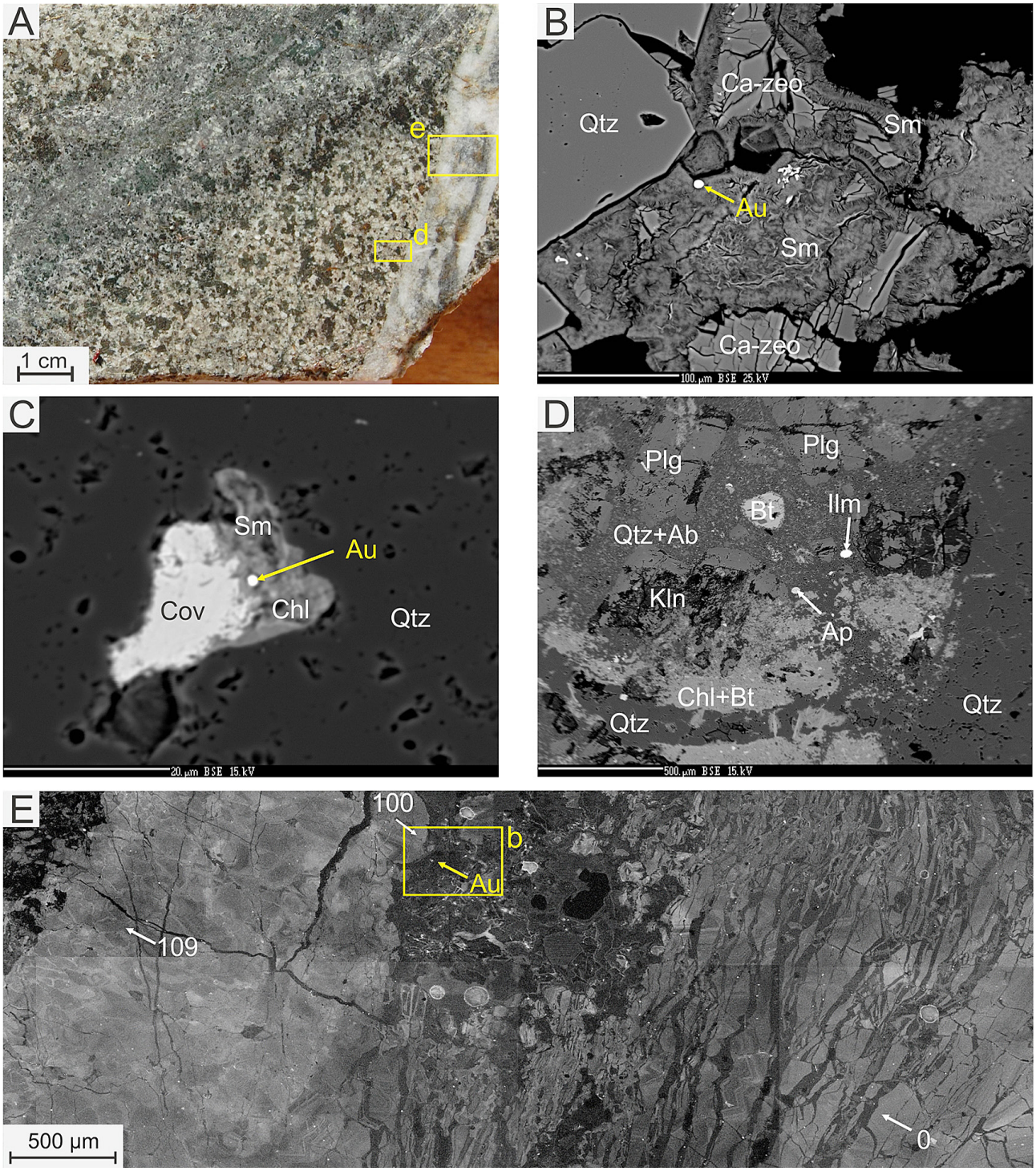

Fig. 8. Images documenting the Beluj gold mineralization (in sample BVE-1/229.2): A – macrophotograph of the core with banded quartz hosting native gold; B – gold hosted by smectite replacing zeolite in a cavity in the quartz veinlet; C – gold associated with chlorite, smectite and covellite in a cavity in the quartz veinlet (BSE); D – detail of rock in the vicinity of quartz veinlet with native gold (shown in A), affected by K-silicate a intermediate argillic alteration (BSE); E – CL image of the quartz veinlet shown in A with location of the gold grain shown in B; arrows with numbers represent spot concentrations of Ti (in ppm).

origin, while their size is up to 5 µm, exceptionally up to 10 µm in diameter. They occur in all types of quartz veinlets. In B-type quartz veinlets, vapour inclusions are most common, sometimes concentrated in irregular bands where they are locally accompanied by magnetite and ilmenite inclusions forming dark bands in quartz of low intensity in CL. Vapour inclusions were studied using Raman spectroscopy, however, most of the inclusion appeared to by Raman inactive, probably due to the small size of inclusions and low density of trapped gases. Just in two primary vapour inclusions hosted by A-type quartz the presence of CO_2 was detected with two characteristic bands at 1286 and 1388 cm^{-1} (Fig. 9a).

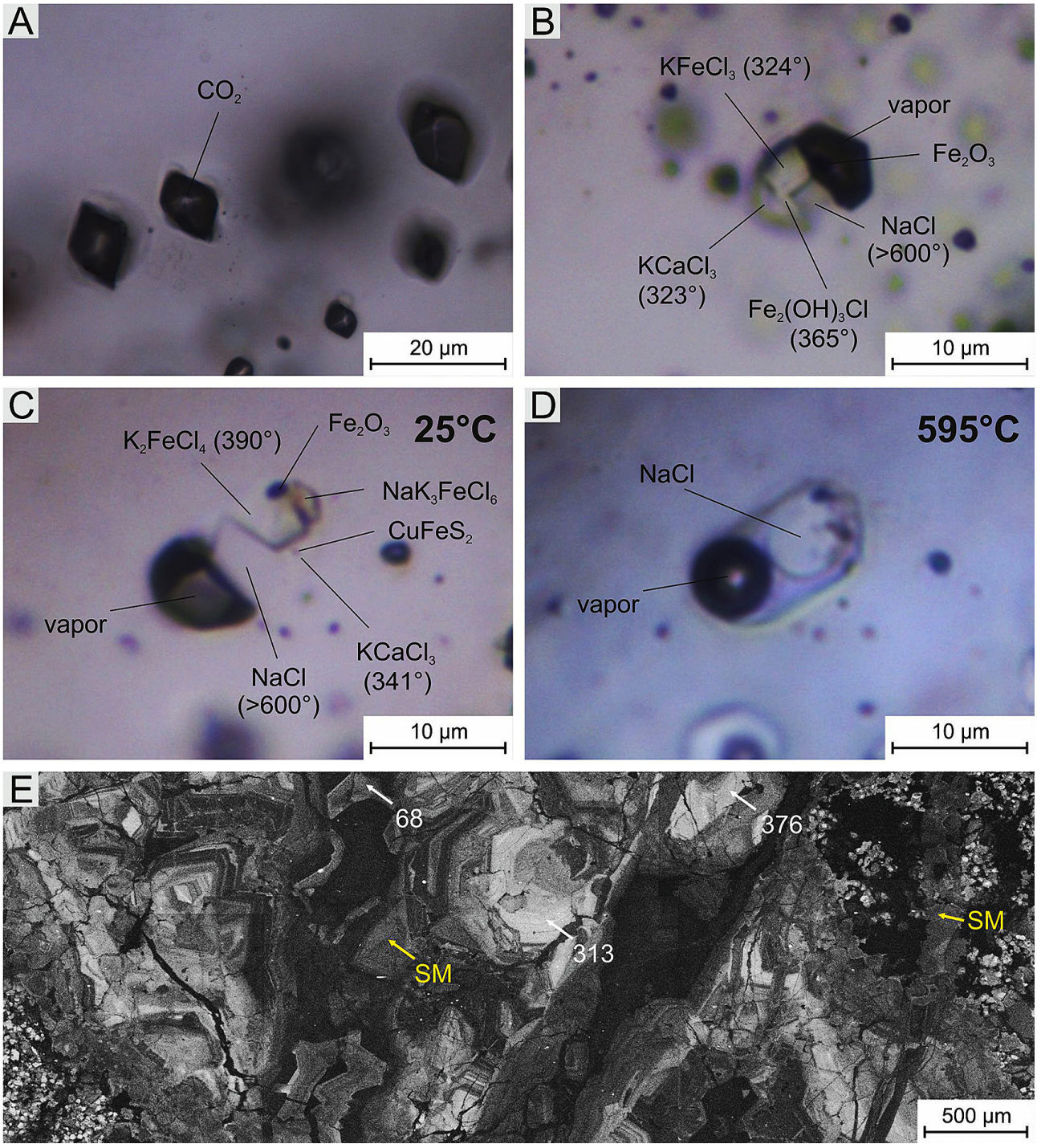

Fig. 9. Microphotographs of fluid inclusions in quartz veinlets in the Beluj site with identification of gases and solid phases by Raman spectroscopy. Also shown are temperatures of dissolution of solid phases in salt melt inclusions: A – primary vapour inclusions with detected CO_2; B – first type of salt melt inclusions; C – second type of salt inclusions; D – the same inclusion as shown in C but at 595°C; note that one of the major solids (halite) still did not dissolve and vapour bubble is still present, but both are smaller than at room temperature; E – CL image of the quartz veinlet hosting salt melt inclusions (SM), arrows with numbers represent spot concentrations of Ti (in ppm; BVE-1/121.3).

Salt melt inclusions are rare type of inclusions containing several solid phases and a distorted vacuole (up to 40 % by volume), but no visible liquid phase at room temperature. They are mostly less than 10 µm in diameter and occur in A-type veinlets in luminescent quartz with a relatively high Ti content (68 ppm; Fig. 9e). Assemblages of inclusions have consistent phase proportions of several salt crystals and are associated with coeval vapour inclusions. Identification of the daughter minerals was based on combination of optical properties, Raman spectroscopic study, microthermometric behaviour and comparison to published data on salt melt inclusions from the Biely Vrch deposit, including Raman spectra

of main Cl-bearing daughter minerals (Koděra et al., 2014, 2015). At the Beluj site two types of salt melt inclusions could be recognized (Figs. 9b, 9c). In the first type, all inclusions contain a dark green anisotropic crystal with a relatively high relief, which sometimes occupies more than half of the volume of these salt melt inclusions. This phase has characteristic main Raman bands at 118, 133 and 235 cm^{-1}, indicative of $KFeCl_3$ (javorieite). This type of inclusions also contain a smaller pale green-yellowish phase with a lower relief than javorieite. Its Raman spectra with main bands at 200, 384 and 3452 cm^{-1} was at Biely Vrch tentatively identified as $Fe_2(OH)_3Cl$ (hibbingite). In the second type, the inclusions contained a green crystal with a high relief, but main Raman bands at 98, 138 and 170 cm^{-1} are indicative of K_2FeCl_4. Another green-yellow phase produced here Raman bands at 168 and 233 cm^{-1} indicative of $K_3NaFeCl_6$. In addition, both types of inclusions also contained at least one or two transparent crystals of similar refractive index as the host quartz, therefore they were often hard to discern, especially in small inclusions. One of the phases was identified as $KCaCl_3$ (chlorocalcite) with main bands at 142 and 147 cm^{-1}. Another transparent low relief daughter mineral of cubic shape was not Raman active and in most inclusions it probably represents halite. Sometimes, some very small opaque phases also occurred in salt melt inclusions, identified based on their Raman spectra as hematite (408 cm^{-1}), sphalerite (350 cm^{-1}) and chalcopyrite (293 cm^{-1}).

Microthermometric study enabled to observe phase changes in the salt melt inclusions during slow heating (Fig. 10). Javorieite was the first phase in inclusions that started to melt on heating in temperature range 323 to 355 °C, sometimes accompanied by dissolution of chlorocalcite, which melted in range 323 to 341 °C. Hibbingite (?) melted at temperatures 358 to 394 °C. The transparent Raman inactive phases with low relief (probably halite) melted in range 406 to 449 °C. In the second type of inclusions, halite was just partially melted at the maximum possible temperature of heating (600 °C), thus its melting temperature is higher than 600 °C (Fig. 9d). The K_2FeCl_4 phase dissolved here at 390 °C, but rinneite probably did not dissolve

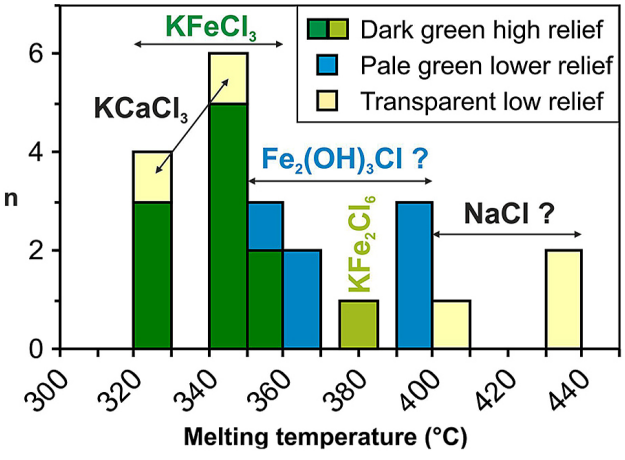

Fig. 10. Frequency histogram of dissolution temperatures of daughter minerals in salt melt inclusions during their heating with identification of probable minerals that have melted in the inclusions (see text for details).

Tab. 4. Chemical composition of salt melt inclusions (SM) and vapour inclusions (V) from Beluj based on interpreted LA-ICPMS analyses. For individual assemblages of fluid inclusions (FI) mean values of element concentrations are shown, assuming the signal for a given element was higher than detection limit. n.d. = concentration below detection limit

FI assemblage	Type of inclusion	Number of FI	$FeCl_2$ (wt%)	Fe (ppm)	KCl (wt%)	K (ppm)	NaCl (wt%)	Na (ppm)	$CaCl_2$ (wt%)	Ca (ppm)	$MnCl_2$ (wt%)	Mn (ppm)	Mg (ppm)	Al (ppm)	S (ppm)	Cu (ppm)	Ag (ppm)	Au (ppm)
BVE-1/119.8 as1	S+V	2	31.2	560	29.8	1250	28.6	450	4.9	2390	5.3	43	290	4190	n.d.	680	180	2.8
BVE-1/119.8 as2	S+V	2	34.0	380	31.6	1100	26.3	240	3.2	2600	4.7	43	200	830	n.d.	25	970	2.5
BVE-1/119.8 as3	S+V	5	35.1	380	30.9	1100	28.1	240	2.7	2600	5.2	43	160	270	n.d.	750	250	2.7

FI assemblage	Type of inclusion	Number of FI	Mg (ppm)	Al (ppm)	S (ppm)	Cu (ppm)	Ag (ppm)	Au (ppm)
BVE-1/119.8 as1	V	9	41	n.d.	n.d.	250	4	n.d.
BVE-1/119.8 as2	V	7	54	n.d.	n.d.	100	n.d.	n.d.

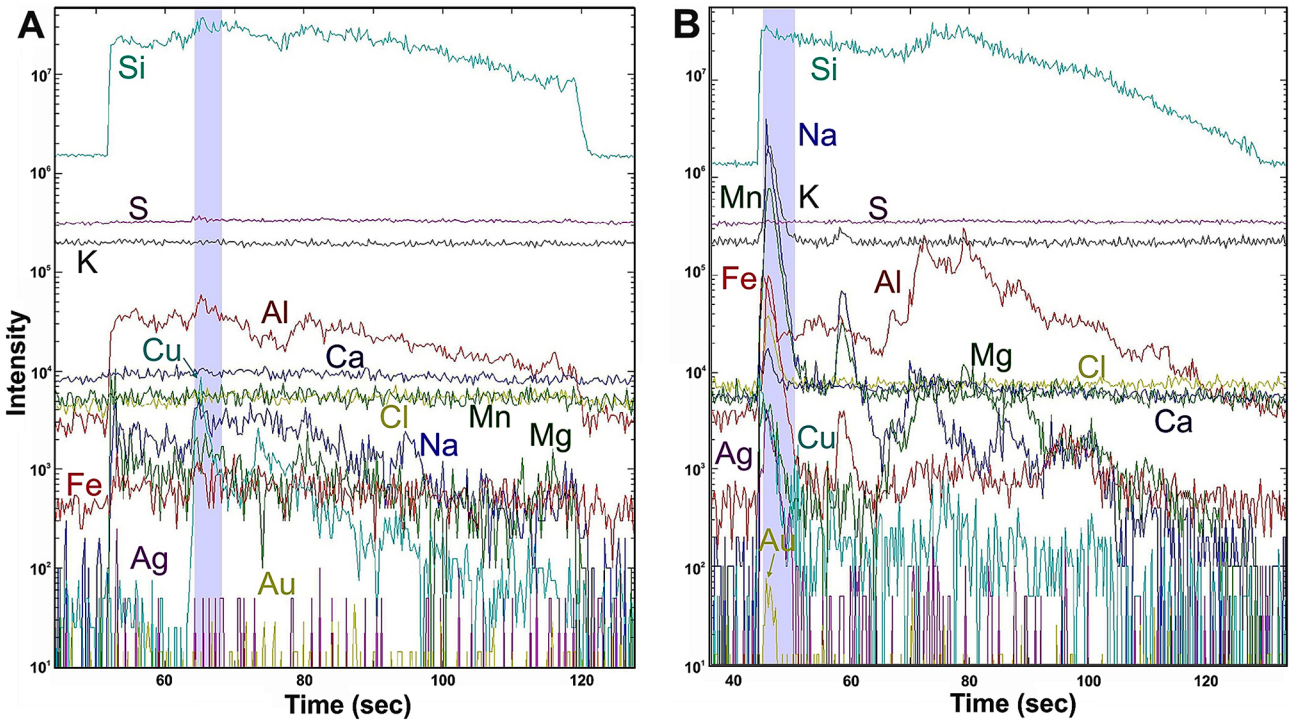

Fig. 11. Example of a transient LA-ICPMS signals obtained from a typical vapour inclusion (A) and salt melt inclusion (B). Grey bands represent that part of the signal when laser has reached and ablated the targeted inclusion.

up to 600 °C. In neither of the studied inclusions heating up to 600 °C has induced liquid-vapour homogenization (Fig. 9d). At this temperature, the vapour bubble still occupied a significant volume of the inclusions, suggesting either much higher homogenization temperatures or some post-entrapment modification of the inclusions (e.g., diffusion of water out of the inclusions or changes in volume of inclusions due beta to alpha quartz transition on cooling).

Two-phase liquid-vapour fluid inclusions were rarely observed in the vein quartz. Most of these inclusions appeared to be primary with variable vapour/liquid ratio, indicative for later, much lower trapping temperatures than the salt melt inclusions, but microthermometric study was not performed on them.

Microanalytical study of chemical composition of salt melt and vapour inclusions by LA-ICP-MS was realized on inclusions hosted by the sample BVE-1/119.8 (Fig. 11, Table 4). Salt melt inclusions were studied on three different assemblages of inclusions, but all of them showed a relatively small variability in chemical composition. The main components of salt melts are $FeCl_2$ (31–34 wt. %), KCl (29–32 wt. %) and NaCl (26–29 wt. %). Minor components include $CaCl_2$ (3–5 wt. %) and $MnCl_2$ (5 wt. %). Concentrations of metals in salt melts are 2.5 to 2.8 ppm Au, 180 to 970 ppm Ag and 25 to 750 ppm Cu. Concentrations of sulphur is below detection limit in all analysed inclusions. Vapour inclusions were studied on two assemblages of inclusions. Despite to their apparent low density, both of them showed systematically increased concentrations of copper (calculated at 100–250 ppm Cu at model salinity 1 wt. %), but neither gold nor sulphur were detected here. Concentration of salts in the inclusions was quite variable, mostly close to detection limit, but generally K seems to prevail over Fe and Na.

4.5. Stable isotopes

Analytical study of oxygen isotope composition was realized on monomineral separates of vein quartz (both A- and B-types) and magnetite from K-silicate alteration. Isotopic composition of vein quartz was analysed from 8 samples from various depths (30 to 244 m), while the observed variation of $\delta^{18}O$ was very small from 9.0 to 9.6 ‰ $\delta^{18}O$ with higher values belonging to A-type veinlets and lower to B-type veinlets (Fig. 12). Three analyses of magnetite from K-silicate alteration from depths 45 to 112 m showed range of isotope compositions from 2.2 to 2.5 ‰ $\delta^{18}O$, following a trend of slight increase of values towards depth. Assuming isotopic equilibrium of quartz and magnetite with the same fluid, quartz-magnetite isotope geothermometry yields 573 °C (Zheng & Simon, 1991) or 651°C (Clayton & Keiffer, 1991). At these temperatures, mean isotopic composition of equilibrium fluids would be 7.3 or 7.9 ‰ $\delta^{18}O$ (Hu &

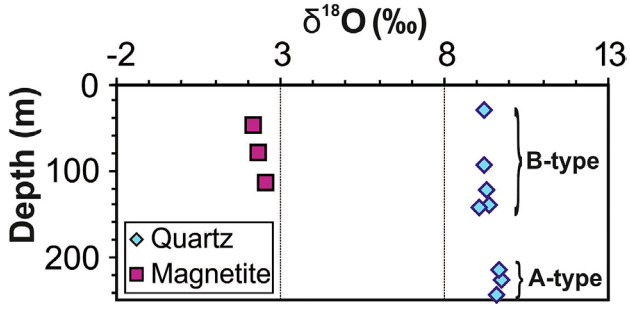

Fig.12. Oxygen isotope composition of vein quartz and magnetite along drill holes BVE-1 and BVE-2.

Clayton, 2003), which are values consistent with magmatic source of fluids (Giggenbach, 1992).

5. DISCUSSION

The new data from the Beluj porphyry gold system enable to compare this system with other porphyry gold system in the Central Slovakia Volcanic Field. Apparently, there are a number of similar properties, including alteration patterns, mineralogy, fluid inclusion and stable isotope data.

The andesite/diorite porphyry at the Beluj system has comparable mineralogical and geochemical composition to other parental intrusions of the porphyry gold systems in the Javorie stratovolcano, indicating a similar source of magma. Mafic medium-K to high-K andesite magmas of the Western Carpathians are thought to result from extension-related partial melting of previously metasomatised and oxidized lithospheric mantle (e.g., Harangi et al., 2007). Such post-subduction setting is known to be favourable for the evolution of Au-rich and Cu-depleted porphyry deposits as the gold is likely to be enriched here by preceding subduction metasomatism and re-melted in an extensional setting (Richards, 2009; Koděra et al., 2014). The presence of rare garnet in the Beluj porphyry is similar to the Kráľová intrusive centre, hosting the porphyry gold occurrence of Kráľová (Hanes et al., 2010).

Hydrothermal alteration zones at the Beluj system are similar to other well studied porphyry gold systems in the Javorie stratovolcano and in the mantle of the Štiavnica stratovolcano. Similar to the Biely Vrch deposit, K-silicate alteration starts to change to Ca-silicate alteration towards depth. However, at the Beluj site these alteration zones geochemically do not show a significant input of potassium or calcium compared to the fresh rock (Koděra et al., 2015). Intermediate argillic alteration is more distinctive but has variable mineral composition and intensity. No zones of Ca-enriched pseudobreccia were found at Beluj to accompany the margins of the hydrothermal system such as that at Biely Vrch (Lexa et al., 2014). Just a local increase in Ca/Na ratio was recognized due to the presence of low temperature Ca-alteration, accompanying the intermediate argillic zones. Similar to the Biely Vrch site, at the Beluj system there occur extensive elongated zones of advanced argillic alteration which are post-mineralization in age and located outside of the mineralized stockwork zone. Thus the studied drill holes did not significantly hit this type of alteration.

The quartz stockwork extent at the Beluj occurrence has a similar composition compared to the Biely Vrch deposit, including EB-, A- and B-type veinlets. However, the spatial extent is significantly smaller (c.f., Hanes et al., 2010). This implies that the magmatic hydrothermal system was of significantly smaller size with a smaller potential to make an economic deposit.

Distribution of gold at the Beluj site is similar to other porphyry gold deposits worldwide, roughly overlapping with the quartz stockwork extent (e.g., Muntean & Einaudi., 2001). Native gold was found only hosted by smectite, which is the product of intermediate argillic alteration. The gold fineness here (891–951) is comparable to gold fineness hosted by intermediated argillic minerals at the Biely Vrch deposit (895–990) or at Slatinské Lazy (785–883; Kozák et al., 2015). At the Biely Vrch deposit, gold in intermediate argillic minerals was interpreted to be secondary, resulting from redistribution of gold from their earlier host – high temperature silicate minerals. Primary gold was found there in hydrothermal plagioclase and amphibole, where it probably precipitated directly from salt melts (Kozák et al., 2015).

Fluid inclusion study has shown that early evolution of the Beluj system was governed by Au-bearing salt melts. As discussed earlier, the origin of salt melts requires a shallow subvolcanic emplacement of a high-K, calc-alkaline magma at high temperature (~850 °C), with intrusion emplacement not deeper than 1 km below the palaeosurface (500 m in the Javorie stratovolcano based on palaeovolcanic reconstruction; Koděra et al., 2014). Thus a similar *p-T* conditions can be also expected for the Beluj system. The unusual gold-bearing Fe-K-rich salt melt inclusions have a similar composition as in other porphyry gold localities in the Central Slovakia Volcanic Field, except of shallow parts of the Biely Vrch deposit. The Biely Vrch deposit is the least eroded system in this field and the upper part of the system contains more Fe-K enriched salt melt inclusions, while the enrichment results from precipitation of halite during ascent of the hot fluid (Koděra et al., 2015). Thus it follows, that the Beluj system has deeper erosion level than the Biely Vrch deposit, but similar to other localities in the Javorie stratovolcano (Kráľová, Slatinské Lazy).

Unfortunately, due to the problematic calibration of the TitaniQ geothermometer in the absence of reliable data on activity of titanium in the parental fluids (Thomas et al., 2010; Huang & Audétat, 2012), we can only roughly estimate the temperatures by comparison with the Biely Vrch deposit where this thermometer was successfully applied (Koděra et al., 2013). At the Beluj site, A-type veinlets contained up to 392 ppm Ti (95 ppm Ti in average), which correspond to temperatures up to 780 °C (570 °C in average) if the calibration from the Biely Vrch deposit is applied. Furthermore, salt melt inclusion microthermometry also indicates that the A-type quartz veinlets hosting the inclusions must have crystallized at high temperatures, exceeding 600 °C at least in some zones of the veinlets. Quartz-magnetite isotope thermometry also confirms such high temperatures (573/651 °C). In contrast, the B-type veinlets have just a low amount of titanium (< 8 ppm), which indicates temperatures below 380 °C.

Interestingly, despite the large difference between crystallization temperatures of both types of veinlets, oxygen isotope data showed only a small difference in $\delta^{18}O$ values, despite the strong sensitivity of quartz-water oxygen isotope fractionation to temperature. The relatively small change can be probably explained by changing isotopic composition of source fluids (more meteoric component in B-type veinlets), which compensated the effect of changing fluid-mineral isotope fractionation at lower temperature. Alternatively, the small difference in isotopic composition of both types of veinlets can be explained by complex textures of veinlets, containing both earlier and later quartz (as seen in CL imaging).

In most porphyry systems, precipitation of intermediate argillic alteration is related to nearly neutral pH fluids linked to

progressive cooling of the system with initial meteoric water incursion that overprints earlier alteration patterns (Sillitoe, 2010). At the Beluj site, these fluids can be possibly linked to rare liquid-vapour fluid inclusions. Advanced argillic alteration, which appears on tops of porphyry systems, generally result from condensation of magmatic vapour and can be linked to a new portion of magma emplaced at depth (Sillitoe, 2010).

LA-ICPMS data from fluid inclusions indicate that the source of gold for the porphyry system in the Beluj site were salt melts coexisting with vapour with increased content of copper but not accompanied by gold and sulphur. This feature is common for all porphyry gold systems in the Javorie stratovolcano (Koděra et al., 2015). After fluid exsolution from the parental magma, copper has apparently preferentially fractionated to vapour while gold fractionated to salt melt. However, due to the low sulphur fugacity, resulting from fluid expansion on ascent to subsurface conditions at high temperature but low pressure, precipitation of copper sulphides was very limited, which explains the gold-only enrichment of this (and other) porphyry gold magmatic-hydrothermal system.

6. CONCLUSIONS

The Beluj magmatic-hydrothermal centre has typical features of porphyry gold systems, such as high Au/Cu ratio, the presence of banded quartz veinlets hosted by small dioritic porphyry intrusions and lack of sulphides but abundant magnetite (Seedorf et al., 2005). Furthermore, they also share several specific properties with porphyry gold systems in the neighbouring Javorie stratovolcano, such as the presence of Fe-K rich salt melt inclusions containing gold and low density vapour inclusions containing copper. Because of the relatively small size of the hydrothermal system, manifested by a limited extent of quartz stockwork, most of the hydrothermal alterations are of relatively low intensity with minor changes in chemical composition compared to the fresh porphyry. Just the late-stage fluids have locally caused significant leaching of sodium and resulted in intermediate argillic alteration. Native gold was found hosted in smectite in cavities of banded quartz veinlets and is interpreted as secondary gold. Primary gold was probably introduced by salt melts resulting from very shallow emplacement of the parental magma. Distribution of alteration zones and composition of salt melt inclusion in comparison with other systems indicates that the erosion level is relatively shallow, but deeper than at the Biely Vrch deposit.

Acknowledgements: Support by EMED Slovakia, Ltd., APVV-0537-10 grant, VEGA 1/0560/15 grant and UK/91/2014 grant are acknowledged. Authors thank J. Zachariáš and an anonymous reviewer for their valuable comments that improved the manuscript.

References

Bakos F., Fuchs P., Hanes R., Žitňan P. & Konečný V., 2010: Au-porphyry mineralization in the mantle of the Štiavnica stratovolcano (Western Carpathians). *Mineralia Slovaca*, 42, 1–14.

Chernyshev I. V., Konečný V., Lexa J., Kovalenker V. A., Jeleň S., Lebedev V. A. & Goltsman Y. V., 2013: K-Ar and Rb-Sr geochronology and evolution of the Štiavnica stratovolcano (Central Slovakia). Geologica Carpathica, 64, 4, 327–351.

Clayton R. N. & Keiffer S. W., 1991: Oxygen isotopic thermometer calibrations. *In*: Taylor, H. P., O'Neil, J. R. & Kaplan, I. R. (Eds): Stable isotope geochemistry: A Tribute to Samuel Epstein. The Geochemical Society, Special Publications, 3, pp. 3–10.

Cox D. P. & Singer D. A., 1988: Distribution of gold in porphyry copper deposits. U.S. Geological Survey Open-File Report 88–46, 22 p.

Eberl D. D., 2003: User´s guide to RockJock – A program for determining quantitative mineralogy from powder X-ray diffraction data. U.S. Geological Survey Open-File Report, 78, 47 p.

Filo M., Bárta R., Kollár Ľ., Kováčiková M. & Pospíšil Ľ., 1980: Vyhľadávací geofyzikálny prieskum belujského intruzívneho komplexu, stredoslovenské neovulkanity. [Geophysical survey of the "Beluj" intrusive complex, Central Slovakian Neogene Volcanics]. Final report for 1978–1980 period. Manuscript, Archive of the State Geological Institute of D. Štúr, Bratislava, 13 p. [in Slovak]

Giggenbach W. F., 1992: Isotopic shifts in waters from geothermal and volcanic systems along convergent plate boundaries and their origin. *Earth and Planetary Science Letters*, 113, 495–510.

Guillong M., Meier D. L., Allan M. M., Heinrich C. A. & Yardley B. W. D., 2003: SILLS: A MATLAB-based program for the reduction of laser ablation ICP-MS data of homogeneous materials and inclusions. Mineralogical association of Canada Short Course 40, Vancouver, B.C., 328–333.

Günther D., Audétat A., Frischknecht R. & Heinrich C. A., 1998: Quantitative analysis of major, minor and trace elements using laser ablation inductively coupled plasma mass spectrometry. *Journal of Analytical Atomic Spectrometry*, 13, 263–270.

Gustafson L. B. & Hunt J. P., 1975: The porphyry copper deposit at El Salvador, Chile. *Economic Geology*, 70, 857–912.

Hanes R., Bakos F., Fuchs P., Žitňan P. & Konečný V., 2010: Exploration results of Au porphyry mineralization in the Javorie stratovolcano. *Mineralia Slovaca*, 42, 15–32.

Harangi S., Downes H., Thirlwall N. & Gméling K., 2007: Geochemistry, petrogenesis and geodynamic relationships of Miocene calc-alkaline volcanic rocks in the Western Carpathian arc, eastern central Europe. *Journal of Petrology*, 48, 2261–2287.

Heinrich C. A., Pettke T., Halter W. E., Aigner-Torres M., Audétat A., Günther D., Hattendorf B., Bleiner D., Guillong M. & Horn I., 2003: Quantitative multi-element analysis of minerals, fluid and melt inclusions by laser-ablation inductively-coupled-plasma mass-spectroscopy. *Geochimica et Cosmochimica Acta*, 67, 18, 3473–3496.

Hu G. X. & Clayton R. N., 2003: Oxygen isotope salt effects at high pressure and high temperature and the calibration of oxygen isotope geothermometers. *Geochimica et Cosmochimica Acta*, 67, 18, 3227–3246.

Huang R. & Audétat A., 2012: The titanium-in-quartz (TitaniQ) thermobarometer: A Critical examination and re-calibration. *Geochimica et Cosmochimica Acta*, 84, 75–89.

Knésl J., Knéslová A., Koděra P., Lexa J. & Michňová J., 2006: Results of exploration for gold at the locality Píla, the Rázdiel part of the Tribeč mountain range. *Mineralia Slovaca*, 38, 3, 202-214. [in Slovak with English summary]

Koděra P., Lexa J. & Konečný P., 2013: Application of CL-imaging and mineral geothermometry on the porphyry gold deposit Biely vrch (Slovakia). *In:* Jonsson, E. et al. (Eds.): 12th Biennial SGA Meeting: Mineral deposit research for a high-tech world. Proceedings, Vol. 2. - I. - Uppsala: Society for Geology Applied to Mineral Deposits, 2013, pp. 817–820.

Koděra P., Heinrich C. A., Fallick A. E., Lexa J. & Biroň A., 2014: Magmatic salt and vapor: Extreme fluids forming porphyry gold deposits in shallow subvolcanic settings. *Geology*, 42, 6, 495–498.

Koděra P., Lexa J., Jánošík M., Brčeková J., Biroň A., Wälle M., Fallick A. E., Kozák J. & Žitňan J., 2015: Hydrotermálne premeny Au-porfýrových systémov v stredoslovenských neovulkanitoch a ich vzťah k vývoju asociujúcich paleofluid [Hydrothermal alteration of Au-porphyry systems in the Central Slovakia Volcanic Field and their relationship to the evolution of accociated paleofluids]. *In:* Jurkovič Ľ, Slaninka I. & Ďurža O. (Eds.): Proceedings from the conference Geochémia 2015, Bratislava, pp. 89–92. [in Slovak]

Konečný V., Lexa J. & Kiripolský J., 1977: Základný geologický výskum a mapovanie v mierke 1 : 25 000, list Prenčov [Basic geological exploration and mapping at the scale 1 : 25 000, sheet Prenčov]. Partial final report. Report No. 42 101, Archive of the State Geological Institute of D. Štúr, Bratislava, 123 p. [in Slovak]

Konečný V., Lexa J. & Hojstričová V., 1995: The Central Slovakia Neogene Volcanic Field: a review. *Acta Vulcanologica*, 7, 2, 63–78.

Konečný V., Lexa J., Halouzka R., Hók J., Vozár J., Dublan L., Nagy A., Šimon L., Havrila M., Ivanička J., Hojstričová V., Mihaliková A., Vozárová A., Konečný P., Kováčiková M., Filo M., Marcin D., Klukanová A., Liščák P. & Žáková E., 1998: Explanations to the geological map of the Štiavnické vrchy and Pohronský Inovec Mountains (Štiavnica stratovolcano). I. and II. part. Bratislava, Geological Survey of Slovak Republic, Bratislava, 473 p. [In Slovak with English summary]

Kozák J., Koděra P., Chovan M., Brčeková J., Lexa J., Bakos F. & Žitňan J. 2015: Distribúcia a zloženie zlata v Au-porfýrových systémoch v stredoslovenských neovulkanitoch [Distribution and composition of gold in Au-porphyry systems in the Central Slovakia Neogene Volcanic Field]. *In:* Jurkovič Ľ, Slaninka I. & Ďurža O. (Eds.): Proceedings from the conference Geochémia 2015, Bratislava, pp. 100–103. [in Slovak]

Lexa J., Koděra P., Onačila D., Rojkovičová Ľ., Žáková E. & Tréger M., 1997: Komplexné hodnotenie prognóznych zdrojov nerastných surovín v oblasti centrálnej zóny štiavnického stratovulkánu [Complex assessment of prognostic resources in area of the central zone of the Štiavnica stratovolcano]. Partial final report. Archive of the State Geological Institute of D. Štúr, Bratislava, 225 p. [in Slovak]

Lexa J., Štohl J. & Konečný V., 1999: Banska Štiavnica ore district: Relationship among metallogenetic processes and geological evolution of the central volcanic zone. *Mineralium Deposita*, 34, 639–654.

Lexa J., Biroň A. & Koděra P., 2014: Nezvyčajné „brekcie" Au-porfýrového systému Biely vrch. [Unusual "breccias" of the Au-porphyry system Biely vrch]. *In:* Jurkovič Ľ, Slaninka I. & Ďurža O. (Eds.): Proceedings from the conference Geochémia 2014, Bratislava, pp. 129–132. [in Slovak]

Macaulay C. I., Fallick A. E., Haszeldine R. S. & Graham, C. M. 2000. Methods of laser-based stable isotope measurement applied to diagenetic cements and hydrocarbon reservoir quality. *Clay Minerals*, 35, 313–322.

Molnár L., Koděra P. & Bakos F. 2012: Au-porphyry mineralization in Beluj (Štiavnica stratovolcano, Slovakia). *Acta Mineralogica-Petrographica*, Abstract Series, 7, p. 90.

Muntean J. L. & Einaudi M. T., 2001: Porphyry-epithermal transition : Maricunga Belt, Northern Chile *Economic Geology*, 96, 743–773.

Richards J. P., 2009: Postsubduction porphyry Cu-Au and epithermal Au deposits: Products of remelting of subduction-modified lithosphere. *Geology*, 37, 247–250.

Roedder E. 1984: Fluid inclusions. *Reviews in Mineralogy,* 12, Mineralogical Society of America, Washington, DC, 644 p.

Rusk B. G., Lowers, H. A. & Reed M. H., 2008: Trace elements in hydrothermal quartz: Relationships to cathodoluminescent textures and in sights into vein formation. *Geology*, 36, 7, 547–550.

Sillitoe, R. H., 2010: Porphyry Copper Systems. *Economic Geology*, 105, 3–41.

Seedorf E., Dilles J. H., Phoffett Jr. J. M., Einaudi M. T., Zurcher L., Stavast W. J. A., Johnson D. A. & Barton M. D., 2005: Porphyry deposits: Characteristics and origin of hypogene features. *Economic Geology*, 100, 251–298.

Sinclair W.D., 2007: Porphyry deposits. *In:* Goodfellow W.D. (Ed.): Mineral deposits of Canada: A synthesis of major deposit-types, district metallogeny, the evolution of geological provinces, and exploration methods. Geological Association of Canada, Mineral Deposits Division, Special Publication, 5, pp. 223–243.

Środon J., Drits V. A., McCarty D. K., Hsieh J. C. C., & Eberl D. D. 2001: Quantitative XRD analysis of clay-rich rocks from random preparations. *Clays and Clay Minerals*, 49, 514–528.

Thomas J. B., Watson E. B., Spear F. S., Shemella P. T., Nayak S. K. & Lanzirotti A., 2010: TitaniQ under pressure: the effect of pressure and temperature on the solubility of Ti in quartz. *Contributions to Mineralogy and Petrology*, 160, 743–759.

Zheng Y. F. & Simon K. 1991: Oxygen isotope fractionation in hematite and magnetite: a theoretical calculation and application to geothermometry of metamorphic iron-formation. *European Journal of Mineralogy*, 3, 877–886.